



HAL
open science

Activation energy for pore opening in lipid membranes under an electric field

Eulalie Lafarge, Pierre Muller, André Schroder, Ekaterina Zaitseva, Jan Behrends, Carlos Marques

► **To cite this version:**

Eulalie Lafarge, Pierre Muller, André Schroder, Ekaterina Zaitseva, Jan Behrends, et al.. Activation energy for pore opening in lipid membranes under an electric field. Proceedings of the National Academy of Sciences of the United States of America, 2023, 120 (11), 10.1073/pnas.2213112120 . hal-04292666

HAL Id: hal-04292666

<https://hal.science/hal-04292666>

Submitted on 21 Nov 2023

HAL is a multi-disciplinary open access archive for the deposit and dissemination of scientific research documents, whether they are published or not. The documents may come from teaching and research institutions in France or abroad, or from public or private research centers.

L'archive ouverte pluridisciplinaire **HAL**, est destinée au dépôt et à la diffusion de documents scientifiques de niveau recherche, publiés ou non, émanant des établissements d'enseignement et de recherche français ou étrangers, des laboratoires publics ou privés.

Activation energy for pore opening in lipid membranes under an electric field

Eulalie J. Lafarge^a, Pierre Muller^a, André P. Schroder^b, Ekaterina Zaitseva^{c,d}, Jan C. Behrends^c, and Carlos M. Marques^{a,e}

^aCharles Sadron Institute, UP22, University of Strasbourg, CNRS, 67034 Strasbourg, France; ^bUniversity of Lyon, CNRS, INSA Lyon, LaMCoS, UMR5259, 69621 Villeurbanne, France; ^cMembrane Physiology and Technology, Institute of Physiology, University of Freiburg, 79104 Freiburg, Germany; ^dIonera Technologies GmbH, 79104 Freiburg, Germany; ^eUniversity of Lyon, ENS-Lyon, Chemistry Laboratory, CNRS UMR 5182, 69342 Lyon, France.

This manuscript was compiled on November 21, 2023

The standard model of pore formation was introduced more than 50 years ago and it has been since, despite some refinements, the cornerstone for interpreting experiments related to pores in membranes. A central prediction of the model concerning pore opening under an electric field is that the activation barrier for pore formation is lowered proportionally to the square of the electric potential. However, this has only been scarcely and inconclusively confronted to experiments. In this paper we study the electropermeability of model lipid membranes composed of 1-palmitoyl-2-oleoyl-glycero-3-phosphocholine (POPC) containing different fractions of POPC-OOH, the hydroperoxidized form of POPC, in the range [0-100] mol %. By measuring ion currents across a 50 μm diameter black lipid membrane (BLM) with picoampere and millisecond resolution, we detect hydroperoxidation-induced changes to the intrinsic bilayer electropermeability and to the probability of opening angstrom-size or larger pores. Our results over the full range of lipid compositions show that the energy barrier to pore formation is lowered linearly by the absolute value of the electric field, in contradiction with the predictions of the standard model.

Electroporation | Pore formation | Electropermeability | Lipid hydroperoxidation

Membrane electroporation, the opening of pores in biomembranes under electric fields, has nowadays become a well established technique in medicine, food processing and biotechnology to permeabilize the membrane of cells thus allowing delivery of drugs and other molecules (1). Despite its clear importance, the physical origin of pore opening by electrical fields is intensely debated and, in defiance of long-standing theoretical and numerical simulation efforts, no unified and quantitative view of the phenomenon has yet emerged. Crucially, the most developed theoretical model for pore opening usually referred to as *the standard model of pore formation* has never been validated or seriously challenged by experimental data, mainly due to the scarcity of experimental efforts designed to test the main predictions of the model (2). This jeopardizes progress in the field, particularly when one considers that every aspect of the widespread phenomenology that relates to lipid membranes with pores refers to or stands on the framework provided by the standard model. In particular, the standard model assumes that pore nucleation under an electric field is a direct consequence of membrane tension changes; since there is evidence that tension depends quadratically on the electric field (3), the model predicts a quadratic decrease of the activation barrier of pore formation with V , the electric potential jump across the membrane – please see table in the Materials and Methods section for all quantities and their units. Results from numerical simulations do provide a molecular view of the first steps of pore formation, but have only very rarely been compared to experiments or developed to a point where an operational model of pore formation can be elaborated (4). In this paper we test the predicted V^2 reduction of the activation barrier of pore formation in lipid membranes assembled from mixtures of POPC and its hydroperoxidized form POPC-OOH.

Lipid oxidation, a natural outcome of metabolic activity under oxygen, impacts the structure and functioning of biomembranes. While a moderate and controlled amount of oxidation is required for signaling and other cell mechanisms, imbalanced generation of oxidized lipid species has been linked to several diseases such as atherosclerosis, diabetes, Parkinson and Alzheimer, and is known to play a role in aging and carcinogenesis (5). In medicine, photodynamic therapy (PDT), removes undesirable tissue through light-induced oxidation as an alternative to surgery. Although oxidation of lipids can be due to several causes, and results in a variety of final chemical transformations, the first step is always the insertion of a dioxygen at the site of an unsaturated bond, resulting in a hydroperoxidized lipid form (6), such as those displayed in Fig. 1. Somewhat unexpectedly it was found that bilayers can be assembled from fully hydroperoxidized lipids, at least for POPC-OOH, which bears one hydroperoxide group per lipid and for DOPC-OOH₂, the hydroperoxidized form of 1,2-dioleoyl-glycero-3-phosphocholine (DOPC), which bears two OOH groups, *i.e.* one per chain. (7) This allowed to better probe the nature of hydroperoxidized lipid bilayers for which much structural information was obtained: hydroperoxidation significantly increases the area per lipid ($\sim 15\%$ for POPC-OOH and $\sim 20\%$ for DOPC-OOH₂) with a concomitant reduction of bilayer thickness; it also weakens the stretching modulus of the bilayers, reducing it for both DOPC and POPC from circa $200 \text{ mN}\cdot\text{m}^{-1}$ to $50 \text{ mN}\cdot\text{m}^{-1}$ (7). These and other measured properties such as membrane polarity and viscosity (8) reinforce suggestions from computer simulations (9, 10) and from X-ray scattering data (11) that the preferential migration to the interface between water and the hydrophobic core of a fraction or of all the hydroperoxide groups is the main driving factor of structural membrane modifications. Given the extent of such conformational changes, it came as a surprise that bilayers from pure POPC-OOH or DOPC-OOH₂ preserve their impermeability to sugars at least over several hours – the typical duration of experiments with giant unilamellar vesicles (GUVs) (7). This brings into question the ability of hydroperoxidized lipid bilayers to maintain gradients of other bio-relevant small particles such as ions (12).

Biomembranes allow water molecules to cross their $\ell \sim 5 \text{ nm}$ -thick barrier with permeability coefficients P_m as high as $P_m \sim 10^{-5} \text{ m}\cdot\text{s}^{-1}$ while being almost impermeable to the majority of hydrophilic solutes (13). For charged species, permeability

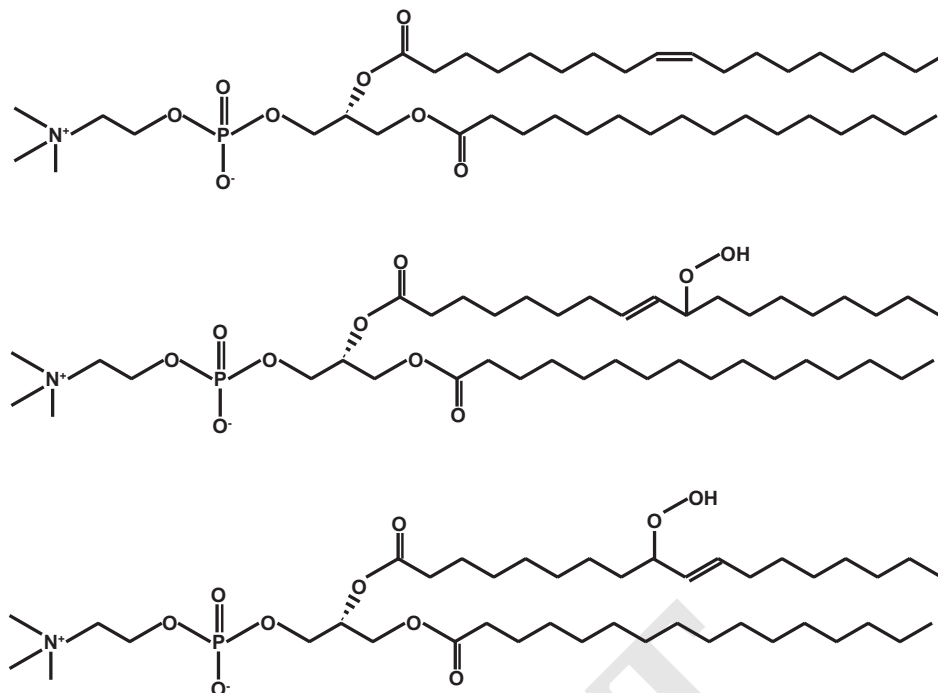


Fig. 1. POPC and POPC-OOH isomers.

is many orders of magnitude smaller at $10^{-12} \text{ m}\cdot\text{s}^{-1}$ for Cl^- , and $10^{-14} \text{ m}\cdot\text{s}^{-1}$ for K^+ , two common bio-relevant ions (14). Permeability values for water and other molecules can be rationalized within a simple picture where a molecule driven by a chemical potential gradient climbs the membrane barrier of free-energy height U_m with probability $\sim \exp(-U_m/k_B T)$, where k_B is the Boltzmann constant and T the absolute temperature, and moves over the barrier top with velocity D/ℓ , thus leading to $P_m = (D/\ell) \exp(-U_m/k_B T)$. With typical diffusion coefficients in oil $D \sim 10^{-9} \text{ m}^2\cdot\text{s}^{-1}$ a molecule takes a few tens of nanoseconds to cross the barrier once it has climbed it (13). For water, the partition coefficient $K_w = \exp(-U_m/k_B T)$, measured often between water and hexadecane is given by $K_w \sim 10^{-5}$ (barrier U_m of order of ten $k_B T$), with correspondingly much smaller values for ions, $K_{\text{Cl}^-} \sim 10^{-12}$ and $K_{\text{K}^+} \sim 10^{-14}$ (and barriers \sim three times larger than for water). As a practical consequence, charge gradients can be indefinitely maintained across lipid membranes, even for large cell-sized lipid vesicles of $R \sim 10 \mu\text{m}$ radius that can equilibrate an osmotic imbalance of $\Delta C \sim 20 \text{ mM}$ within a thousand seconds ($\tau_w \sim R/(P_m \nu_w \Delta C) \sim 1000 \text{ s}$), with ν_w the water molar volume.

In our quest to understand charge transport across lipid membranes, we performed experiments in a black lipid membrane (BLM) geometry – see Fig. S1, carefully identifying and quantifying charge transport events and determining ionic permeabilities in membranes assembled from POPC/POPC-OOH mixtures in a solution of 100 mM KCl. For all bilayers we witnessed the emergence of angstrom-size single pore opening as the field strength was increased, thus allowing to quantify the influence of the field strength on the probability of initial pore formation. Our results do not only bring a new and extensive set of data to the field of electroporation, but also challenge some of the prevailing views in the field.

Significance Statement

Why does a pore open when a high enough electric field is applied to a lipid bilayer? Despite almost a century of efforts we do not have a clear answer to this question, in part due to scarcity of data from experiments designed to probe this phenomenon. Here, we report results from electroporation experiments on black lipid membranes assembled from different mixtures of a common lipid, POPC, and its hydroperoxidized form POPC-OOH. By carefully identifying pore formation events, we were able to quantify the influence of the applied electric field and of the hydroperoxidation degree on the frequency of pore opening. Our results disagree with the standard model of pore formation and bring new significant insight into the factors controlling pore opening under an electric field.

E.J.L. and E.Z. performed experiments. E.J.L., P.M., A.P.S. and C.M.M. analyzed data from experiments. A.S., P.M., J.C.B. and C.M.M. designed and conducted the project. E.J.L., A.S. and C.M.M. wrote the paper. All authors interpreted the data and commented and reviewed the manuscript.

J. C. B. is co-founder and shareholder of Nanion Technologies GmbH, Munich, Germany. J. C. B. and E. Z. are co-founders and shareholders of Ionera Technologies GmbH, Freiburg, Germany.

²To whom correspondence should be addressed. E-mail: carlos.marques@ens-lyon.fr

Results

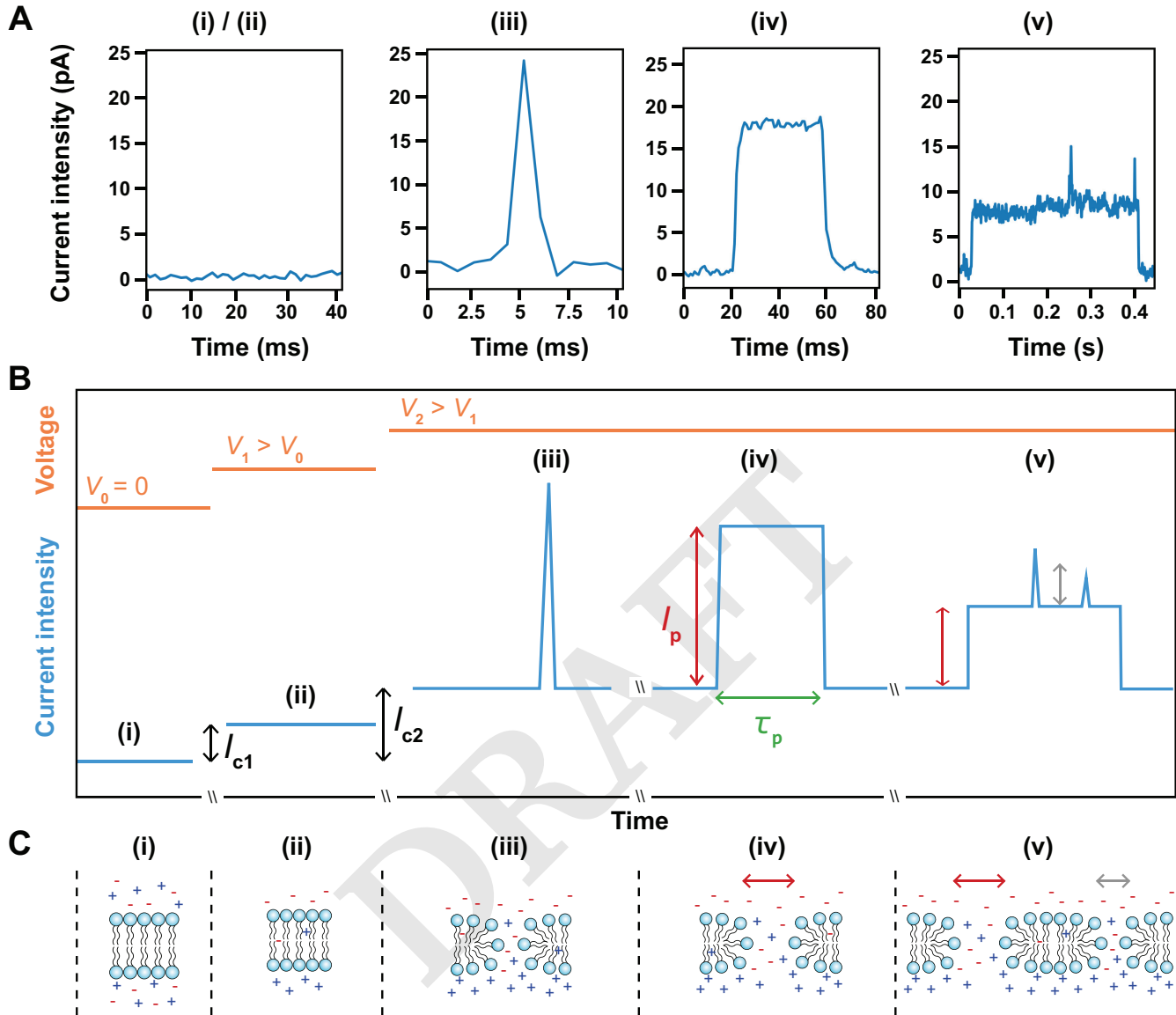


Fig. 2. Current traces and associated membrane geometry. (A) Identifiable segments of $I(t)$ along with (B) their schematic representation and (C) their presumed membrane conformation. Under no (i) or small (ii) applied voltages, the current fluctuates smoothly about a small (\sim pA) average current. Charges accumulate on both sides of the membrane that acts as a capacitor, a small amount of ions cross the membrane. Under larger applied voltages, the opening of short lifetime pores (iii) and long lifetime pores (iv) can be detected by the sudden rise of the current. Pores can accommodate lipid heads along the pore rim, in a conformation referred to as hydrophilic pores. Small numbers of simultaneous pores still allow for identifiable membrane geometries (v).

Our experiments focus on the analysis of the ionic current crossing phospholipid membranes composed of various mole fractions (X_{OOH}) of POPC-OOH. In the following we will first describe and characterize conduction events as a function of applied voltage and hydroperoxidation degree and determine membrane ability to withstand the electric field without rupturing. We then perform a quantitative analysis of intrinsic (pore-free) electropermeability. Finally we quantify the membrane propensity to open pores as a function of applied voltage, identifying the opening of single pores, and studying their characteristic lifetimes, intensities and frequency of formation.

Traces of electric current. In our experiments, the information on charge transport is contained in the time series of the measured current $I(t)$ for a given applied voltage, see Fig. S2 for our voltage ramping protocol and Fig. S3 for the equivalent electric circuit. Given the typical values for the membrane capacitance in the picofarad range – see Fig. S4 for measured values – and the series resistance of order of a few tenths of a megohm, the response time of the equivalent electric circuit is a few microseconds, see sections S3 and S4. Thus, relaxation phenomena in our traces, associated for instance with the decay time τ of the capacitance peaks and current increase after pore opening, is a result of the filtering process implemented in the

recording apparatus and in the software, typically on the order of a few milliseconds, $\tau \simeq 2.7$ ms, see Fig. S5 for filtering and Fig. S6 for chosen examples of current traces.

Fig. 2 proposes a classification of conductance events based on the shape of the observed current fluctuation and assigns each class to a hypothetical mechanism on the level of membrane structure and dynamics. The average current that we designate as I_c is present in all traces. In the absence of an applied voltage V , one has $I_c = 0$; the membrane simply separates two volumes of the ionic solution. When a voltage V is applied the membrane acts as a capacitor of a few picofarad with a “leakage” current I_c of order of several picoamperes. The lipid bilayer bears thus, under an applied potential of 100 mV, roughly one charge per $\simeq 200$ nm² corresponding to 350 lipids. The same area also lets one charge per second cross the membrane barrier.

Sections (iii) and (iv) of Fig. 2 show current fluctuations when a large enough V induces a sudden rise of the current above its baseline value I_c , reaching a maximum and then immediately – case (iii) – or after a plateau phase – case (iv) – returns to the baseline. This is the signature of pore opening, the number of charges conveyed through a pore being a function of the applied voltage, of the ion concentration in the solution and, importantly for the interpretation of the results, of the pore size. Under our conditions, for an applied voltage of 100 mV, a simple conduction model (15) predicts that a pore of $D_p = 1$ nm diameter generates a stationary current I_p of 20 pA with intensity values I_p for pores of different sizes scaling as $I_p \propto D_p^2$. Since pore opening and closing is much faster than the characteristic instrument response time τ , model variations for pore opening can be taken as square gate functions for $D_p(t)$ such as $D_p(t) = D_p$ for $t_i < t < t_i + \tau_p$ and $D_p(t) = 0$ otherwise, with t_i and τ_p the pore initial time and lifetime, respectively, see also Fig. S4. Section (iii) shows an example of short pore, *i.e.* $\tau_p < \tau$, while section (iv) shows the opposite example of a long-lived pore where $\tau_p \gg \tau$ and thus a stationary plateau can be reached before the pore closes, see also section S3. Section (v) of Fig. 2 shows a more complex signal where individual events are nevertheless still *identifiable*. We name trace segments *complex* when the state of the membrane cannot be inferred from the current traces.

Membrane rupture under an applied voltage. As explained before, experiments were performed by ramping up V as shown in Fig. S2. Voltage values at which membrane breakage occurred were collected and averaged to build the membrane survival probability under an imposed voltage - see Fig. S12. While pure POPC membranes (0 % -OOH) have a 50 % probability of breaking at 300 mV in a time span of six seconds, both for positive and negative applied voltages, for nearly fully hydroperoxidized membranes (96 % -OOH), the 50 % rupture probability is reached at 175 mV. Hydroperoxidation, as we will below quantify for all investigated phenomena, renders the membranes increasingly vulnerable to electric fields.

Membrane intrinsic conductivity. If one pictures the lipid membrane as a one dimensional barrier restricting ionic mobility in the direction perpendicular to the bilayer, the standard formulations by Goldman, Hodgkin and Katz (13, 14, 16, 17) can be used to predict the ion current density $i_c = I_c/S$ where S is the effective membrane area contributing to the electric measurement (that we infer from the measured capacity) and I_c is the current measured on *all trace sections devoid of pores*. A simple step-like potential that depends only on the barrier height U_m and on the barrier thickness ℓ leads to a linear relationship between the current and the applied potential. Current-voltage relations $i_c(V)$ with a supralinear component can be obtained from barrier functions of a more complex shape. The simpler of these is the trapezoidal barrier, where the basis of the barrier has thickness ℓ while the top of the barrier at height U_m is thinner, with thickness $b \leq \ell$ (18). Conductivity predictions from the trapezoidal barrier can be written as a cubic expansion of the applied potential:

$$i_c = e c P_m u \left(1 + \left(1 - \frac{b^2}{\ell^2} \right) \frac{u^2}{24} \right) \quad [1]$$

with $u = eV/(k_B T)$, e the elementary charge and c the ion concentration.

Fig. 3 A presents $i_c(V)$ data and fitted curves for all the hydroperoxidation degrees. Results are plotted as a function of both the normalized voltage u and the actual voltage V . For better comparison with results from the literature we provide two Y-axis scales, for both the measured current density (left) and the current crossing a membrane with 42 μm diameter, the average diameter of our membranes as inferred above from capacity measurements.

Eq. (1) fits well the data over a voltage range (shown by full lines in the figure) that depends on the peroxidation degree but that is always large enough to allow for determination of the two fitting parameters, the permeability P_m and the ratio b/ℓ . P_m for pure POPC is measured at $2.8 \pm 2.5 \times 10^{-12}$ m.s⁻¹, consistent with reported permeability values for the anion Cl⁻ that dominates charge transport across the lipid membrane (14). Values of P_m increase steadily with the peroxidation level, as shown in Fig. 3 B, up to $11 \pm 9 \times 10^{-12}$ m.s⁻¹ for the fully hydroperoxidized bilayer, an increase of roughly a factor 4 of the average values. Fittings return an almost constant value for the ratio $b/\ell = 0.87 \pm 0.05$, typical for values reported in the literature for lipid membranes (19). As stated above, membrane permeability is well described by $P_m = (D/\ell) \exp(-U_m/k_B T)$. Observed changes of membrane permeability cannot be explained by the small decrease ($\sim 20\%$) of membrane thickness ℓ (11), and it is unlikely that the diffusion coefficient D of the ions across the membrane increases dramatically with hydroperoxidation, given the small volume fraction occupied by the added organic hydroperoxide. The observed increase is thus better interpreted as due to a lowering of the membrane barrier potential $\Delta U_m = -1.4 k_B T$, at least with respect to anion Cl⁻ that dominates transport here, consistently with the known increase of polarity of the inner membrane region (20).

Pore formation correlates with changes in the barrier to ions. As V increases, the traces show the emergence of ionic transport across the membrane through pores, as depicted above in sections (iii), (iv) and (v) of Fig. 2.

We evaluate first the probability for a membrane to remain free of pores during the six seconds when a constant voltage is applied. Fig. 4 shows this probability for each membrane composition. As the figure shows increasing X_{OOH} results, at any

imposed voltage, in an increase of the probability for the membrane to create pores. For instance, hardly any pore can be detected for pure POPC membranes at applied voltages lower than 50 mV, while for the same voltage in a half of the 96 % POPC-OOH membranes at least one pore was observed. Interestingly, the range of voltage over which Eq. (1) fits well data in Fig. 3 A correlates with voltages at which pore opening probability reaches values higher than 0.90 – see Fig. S13. Thus, the trapezoidal model behind Eq. (1) stops to be valid when the electric fields are high enough to bring the membrane to the verge of pore opening conditions.

Lifetime distribution of identifiable pores. We developed a *threshold method* – see section S7 – to detect identifiable pores with a well defined opening and closing current jump. Using the results from this pore-detection routine we built the distribution of pore lifetimes τ_p displayed in Fig. 5. Since no variation of pore lifetimes was observed with applied voltage (Fig. S14), the results in Fig. 5 are computed by grouping all pores detected for a given -OOH composition irrespective of voltage.

The distribution of lifetimes is shown in Fig. 5 with 0.8 ms time bins. As the figure shows, there is no noticeable difference in the distributions for the various peroxidation degrees. If one excludes the first bin that is at the limit of time resolution, the combined distribution follows a single exponential decay with a time constant of 1.8 ± 0.1 ms (error computed from a 90 % confidence interval of the fit), similar to experiments recorded with 1 ms time resolution under BLM geometry in 100 mM KCl for diphtanoylphosphatidylcholine (DPhPC) membranes (21). It is remarkable that the lifetime is independent of X_{OOH} , suggesting that for these pores, lifetime is determined by phenomena extrinsic to the lipid bilayer. Indeed, as we recently showed (8), hydroperoxidation impacts both the chain and the head region of the membrane, making it unlikely that intrinsic bilayers contributions to the lifetime would be independent of hydroperoxidation degree. A relevant remark in this context is that at the pore site the flow of charges creates an inhomogeneous electric field: the electrical potential difference across the membrane is strongly lowered close to the pore – it would vanish in the center of the pore for the case of a free flow of charges (22) – and it recovers far from the pore to its homogeneous value. Charge rearrangement must therefore take place laterally also, a process with a characteristic time that depends on the size of the region that is perturbed by the flow. This certainly calls for further modeling efforts of the electrical stresses acting on a membrane in the presence of pore flow.

In the following, we discriminate between short and long-lived pores, as defined in section S4, in order to better determine their characteristics and abundance.

Size of short lifetime pores. Given the average lifetime of short-lived pores $\bar{\tau}_p = 1.8 \pm 0.1$ ms obtained by the *threshold method*, most of the pores detected in this category cannot reach a stationary conducting state which requires that the lifetime of the pore τ_p is larger than τ , the time needed to reach the stationary value I_p . It is nevertheless possible to obtain I_p values as explained in section S3. Corresponding values of pores sizes can be computed (15) from $D_p = (4bI_p/\pi V\sigma)^{1/2}$ with $b = 5$ nm the length of the pore and σ the solution conductivity, $\sigma = 1.29 \text{ S}\cdot\text{m}^{-1}$ for a 100 mM KCl solution (23). We obtained an average diameter $\bar{D}_p = 6.4 \pm 2.0 \text{ \AA}$ independently of applied voltage and hydroperoxidation degree, comparable to the lower range of reported radii (4, 21, 24, 25), see also Fig. S16.

Opening frequency of short lifetime pores. We measure the frequency of detection of short lifetime pores using the *threshold method* mentioned above. Fig. 6 A shows the opening frequency of short lifetime pores expressed as the average number N_s of pore openings detected per second for a given applied voltage. As the figure shows, the frequency increases with both voltage and X_{OOH} .

The semi-logarithmic representation of Fig. 6 A reveals a nearly linear dependence of $\ln N_s$ with applied voltage for all the samples, with an almost identical slope for all X_{OOH} . This suggests that under our conditions, frequency of pore opening follows the empirical relation:

$$N_s = f_p |u| \exp(\alpha |u|) \quad [2]$$

with all the information on X_{OOH} being carried by f_p alone. The master curve in Fig. 6 B was obtained by finding $f_p(X_{\text{OOH}})$ values that minimize vertical distance in the semi-logarithmic representation of all curves with respect to $X_{\text{OOH}} = 0$. Fits of this master plot give the pair of values ($\alpha^+ = 0.50 \pm 0.05$, $f_p^+(0) = 1.1 \pm 0.1 \times 10^{-3} \text{ s}^{-1}$) and ($\alpha^- = 0.56 \pm 0.06$, $f_p^-(0) = 1.5 \pm 0.1 \times 10^{-3} \text{ s}^{-1}$) for respectively the positive and the negative branches (errors from a 90 % fit confidence interval). Fig. S19 displays the influence of X_{OOH} on the frequency f_p , which shows both the positive and negative branches are well described by the function $\ln(f_p(X_{\text{OOH}})/f_p(0)) = -1.2 + 0.055 X_{\text{OOH}}$ for all points except the first.

The number of short lifetime pores that we detect is a function of applied voltage and hydroperoxidation degree. The voltage dependence that we observe does not follow the predictions of the standard model for pore formation in lipid bilayers, nor those from the many variants of the model (2, 24, 26, 27). Central to those predictions, is the dependence of the activation barrier for the pore creation rate with V^2 , the square of the applied potential. Incidentally, to our knowledge, this dependence has never been confirmed. Scarce data exists (21) that has been interpreted as a proof of such quadratic variation (28), but a strong confirmation of this effect has not been reported. Our empirical form Eq. 2 suggests rather a direct dependence of the attempt rate with the voltage and an activation energy that is lowered proportionally to $|V|$. Such dependence has been reported in a publication combining experiments and numerical simulations, and qualitatively discussed in terms of the action of the field on the dipolar state of the lipids (4). If we interpret our observations within this frame and estimate the field strength by V/ℓ , the effective dipolar moment μ lowering the pore nucleation barrier is $\mu = \alpha e \ell$ where α is the coefficient in Eq. 2, e the elementary charge and $\ell = 5$ nm the membrane thickness. Given the value provided by our experiments $\alpha = 0.5$ and the (non-SI but widely used) measure of dipolar strength strength by a Debye unit $D = 0.02 \text{ nm}\cdot e$, we get $\mu = 125 D$, one order of magnitude

larger than values reported from simulations (4). A similar analysis performed on data (21) from DPhPC membranes gives $\alpha = 0.42$, denoting a slightly smaller sensitivity of these bilayers to the formation of pores under an applied electric potential.

The voltage effect on the pore formation rate is not, in our experiments, a function of hydroperoxidation degree, contrary to the pore formation rate itself, which dependence on X_{OOH} is shown in Fig. S19. Thus, a fully hydroperoxidized POPC bilayer sees its activation barrier for pore formation lowered by about $5 k_{\text{B}}T$, with a roughly linear dependence on X_{OOH} . Simply put, full hydroperoxidation lowers the barrier for pore formation by as much as an electric field of ~ 250 mV, a rule of thumb that would be interesting to correlate with the molecular transformations induced by the insertion of the -OOH group in the POPC unsaturated chain (10, 29).

Long lifetime pores. Currents associated with large lifetime pores $\tau_{\text{p}} \gg \tau$ reach a stationary value which, despite the ever present fluctuations, provides a clear distinct visual aspect to the traces. They evoke the signature of currents carried by ionic channels, which correspond in general to rather long lived pores of a well-defined size (30). In practice, we developed a *squared gating method* – see section S7 – to filter the signal $I(t)$ in order to remove noise, short lifetime pores and complex signals. Long-lived pores are much scarcer than short-lived pores – see also Fig. 5; thus pore sizes and lifetimes collected for these pores have a larger statistical uncertainty that does not allow, in particular, to assert the influence of voltage or oxidation degree on the frequency of pore opening. We did not find any statistical support for asserting that pores open with a fixed size – and thus conduct a fixed current – for membranes of a given composition. There is rather a disperse distribution of currents, from where an average value can nevertheless be extracted. Significantly, the average current values follow a linear relation with applied voltage, thus enabling to compute an average pore conductance corresponding to an average pore size of $\bar{D}_{\text{p}} = 7.4 \pm 2.8 \text{ \AA}$, a value close to the one found for short lifetime pores. We did not find either a statistically significant variation of average currents with oxidation degree. The lifetime distribution of pores lasting more than 20 ms show, similarly to short lifetime pores, an exponential decay with however a different time constant of 160 ms, see Fig. S18.

Conclusion

By studying conductive events across several hundreds of membranes with different hydroperoxidation degrees and by detecting and analyzing many thousands of those events, we contribute to the discussion about pore formation in lipid membranes with a new set of statistically relevant data that challenges the widely accepted V^2 dependence of the reduction of the barrier for pore nucleation and brings fresh insight to the field.

Our first finding is that the pores start opening at a voltage where the barrier model describing the intrinsic permeability of the membrane to ions stops being valid. Indeed, for low enough voltages the membrane maintains the nature of its permeation barrier to the ions, well described in our case by a trapezoidal model with two lengths and one height. Such barrier corresponds to the molecular organization of the bilayer in the absence of an applied potential. When the pore formation probability becomes finite at high enough voltages, the permeation barrier changes, implying that the lipid organization in the bilayer has changed as well. This validates numerical simulations approaches where the state of the lipids is carefully tracked, for instance with respect to their polarization state, before opening of pores is detected.

For the large majority of events that we detected, the pore lifetime is independent of membrane oxidation. This points to explanations of pore lifetime extrinsic to the lipid membrane such as those related to the lateral relaxation of the electric stresses at the pore site, calling for further studies on the electro-dissipation effects in conductive pores in lipid bilayers (22), and thus challenging whether a configuration walk in a free-energy landscape can capture the essentials of this phenomenon.

Most of the pores that we detected had small diameters, around 0.7 nm, independently of voltage or hydroperoxidation degree. The survival of such small pores over milliseconds or more suggests that they correspond to the so called hydrophilic pores: indeed, lipid head re-organization allowing for the head-carpeting of the inner pore canal is expected to occur tens of nanoseconds only after a water channel nucleates across the membrane (31). Geometrically, such robust result indicates also that these pores adopt the smallest possible diameter compatible with the constraints of lipid packing in the semi-toroidal inner pore surface, also supporting the anticipated deviation at small diameters of the pore line tension from its constant value.

Our results rule out a key prediction from the standard model of pore formation, namely that the barrier for pore nucleation is reduced proportionally to V^2 . Indeed this would imply an increase of the number of pores formed during a given period of time as $\sim \exp(\text{constant} \cdot V^2)$. Under our experimental conditions we observe instead a growth with the electric potential of the form $\sim \exp(\alpha|V|)$. Although this is compatible with explanations based on the field effect on the lipids electric dipoles, we find a dipolar moment one order of magnitude larger than those extracted from simulations. We anticipate much fruitful future developments along these lines to better decipher the molecular forces and membrane properties that control pore opening.

Finally, our results reinforce the picture that has been unraveling over the last decade to describe hydroperoxidized lipid membranes: despite the strong molecular modifications that induce a larger area per lipid, a smaller thickness and a weaker stretching modulus, we find that these membranes retain their integrity, even under an applied electric potential. The work in this paper further shows that hydroperoxidized bilayers behave in a quantitatively different yet standard manner with respect to electropermeation and pore formation: they display a four-fold larger permeability with respect to the anion Cl^- , and open pores with a larger frequency at weaker electric fields.

Materials and Methods

Materials. 1-palmitoyl-2-oleoyl-glycero-3-phosphocholine (POPC, 16:0-18:1) was purchased in chloroform ($25 \text{ mg}\cdot\text{mL}^{-1}$) from Avanti Polar Lipids. Lipids were stored at -20°C and used without further purification. 1,9-Dimethyl-Methylene Blue (MB), KCl, KOH and Hepes were provided as powder from Sigma Aldrich. Cellulose membrane dialysis tubing with a molecular cut-off of 14000 Da and octane are also bought from Sigma Aldrich. All NMR analysis were performed in 99.8 % deuterated methanol (MeOD) supplied by Acros Organics. 10 μL pipettes tips, provided from STARLAB, were used to paint the free-standing lipid membranes.

Lipid hydroperoxydation. Batch solutions of POPC from fresh, *i.e.* sealed, POPC vials, were systematically controlled by NMR before the hydroperoxydation procedure. The two hydroperoxydized isomers of POPC-OOH shown in Fig. 1, were synthesized photochemically using MB as a photosensitizer. Briefly, 6 mL of a MeOD solution of POPC at $5 \text{ mg}\cdot\text{mL}^{-1}$ (6.6 mM) containing MB at $20.8 \mu\text{g}\cdot\text{mL}^{-1}$ ($50 \mu\text{M}$) were placed inside a home-made device composed of red LEDs ($\lambda=625 \text{ nm}$, $600 \text{ W}\cdot\text{m}^{-2}$), under a constant dioxygen flux and stirred for 10 min. Resulting conversion rates ($97 \pm 3 \text{ mol } \%$) were monitored by ^1H NMR. MB, the photosensitizer, was removed by a 4 h dialysis in water. The obtained lipid in water solution was dried and lipids redispersed in MeOD to perform a NMR control. Hydroperoxydized lipid solutions were kept in MeOD at -20°C for further use.

Mixtures of POPC and POPC-OOH. MeOD solutions of POPC and of POPC-OOH were mixed as required to obtain the three targeted values of 25, 50, and 75 mol % of POPC-OOH. For each mixture, the exact POPC-OOH fraction was checked by ^1H NMR, always within $\pm 5 \text{ mol } \%$ of the target value. Solvent was then evaporated, and dried lipids were dissolved in octane at $10 \text{ mg}\cdot\text{mL}^{-1}$. Pure POPC and pure POPC-OOH samples were prepared in a similar manner. Lipids in octane solutions were kept at -20°C and used within a few weeks. Here below, results are grouped by number weighted averages of the measured OOH content.

The measurement device. Experiments were performed on an Orbit Mini miniaturized bilayer workstation (Nanon Technologies, Munich, Germany), with an inserted microelectrode cavity array (MECA 4) recording chip (Ionera Technologies, Freiburg, Germany) as shown in Fig. S1. The chip contains four wells with diameter $50 \mu\text{m}$ and depth $30 \mu\text{m}$, each cavity corresponding to a recording channel. A chloridized silver microelectrode (Ag/AgCl) is present at the bottom of each well and a single, macroscopic common counter electrode is found at the top of the chip.

The Orbit Mini operates in voltage-clamp mode using the Elements 4 (e4) channel-amplifier (Elements SRL, Cesena, Italy). Voltage can be imposed to only selected channel(s), but with a common value, in the range -500 mV to $+500 \text{ mV}$. The current intensity across each well $I(t)$ is measured independently, allowing in principle to record simultaneously the current across four different membranes. However, since the current saturation due to a membrane rupture in one of the channels induces artifact signals in the neighboring channels of the e4 amplifier, we chose to work with a single well at a time. $I(t)$ was measured with a sampling rate of 1.2 kHz and bandwidth 0.6 KHz. The Orbit Mini is piloted by elements data reader 3 (EDR 3) software, offering several measurement gains. Capacitance C_m determination uses a predefined instrument routine working with the $[-20, 20] \text{ nA}$ measurement gauge. We acquired all current signals with the smallest gain, within the range $[-200, 200] \text{ pA}$.

Free standing bilayer preparation. Experiments were conducted at room temperature ($\approx 20^\circ\text{C}$). The MECA 4-chip was filled with $150 \mu\text{L}$ of a fresh buffer solution composed of 100 mM KCl and 10 mM HEPES in milli-Q water, adjusted to pH 7 by addition of 1 M KOH solution, typically $10 \mu\text{L}$ for a total of 5 mL solution. Special attention was given to the complete air removal from each of the four cavities. A bilayer was painted on the top of the cavity by the air bubble method described elsewhere (32). Briefly, an air bubble is formed above the chosen cavity with a $10 \mu\text{L}$ micropipette tip previously immersed in the lipid-in-octane solution. Contact with the well and further removal of the air bubble leaves attached to the rim of the aperture a thin octane film stabilized by lipids. Molecular forces lead to the thinning of the film, resulting – as schematically depicted in Fig. S1 – in a free standing bilayer of area S in the center of the well, surrounded by a thick oil annulus attached to the rim (33). Presence, stability, and quality of the free standing bilayer were monitored with EDR 3 under the application of $\pm 20 \text{ mV}$: a negligible current ($< 0.1 \text{ pA}$) was seen when a sealing membrane was formed, while a saturated current ($\pm 200 \text{ pA}$) was displayed otherwise. When formed, the membrane was left to equilibrate for at least 1 min while continuously checking the stability of the current. In case of an unstable current, the membrane was destroyed and reformed. Afterwards, membrane capacitance C_m was measured. Capacitance variability was observed, we found that reproducible measurements were obtained for membranes with a stable capacitance ranging from roughly 6 to 13.5 pF.

Conductance measurements. Once a membrane was formed, EDR 3 software was used to follow and record current intensity traces $I(t)$ for various imposed voltages V . A defined protocol for increasing applied voltages was applied as shown in Fig. S2. The protocol was manually stopped at membrane rupture, corresponding to sudden irreversible current saturation. If ever a membrane resisted until reaching the sequence where $V = 500 \text{ mV}$, it was not considered as a valid bilayer and the experiment was discarded. The EDR 3 functionalities were first used to manually acquire a small fraction of our data, before acquisition was fully automatized with a home-written macro (Pulover's Macro Creator).

We acquired currents from more than 50 membranes of each targeted lipid composition: 95 membranes for POPC containing 0 % of POPC-OOH, 94 for 25 %, 53 for 50 %, 76 for 75 %, and 55 for 100 %. Statistical analysis of our data required the development of homemade Python scripts implemented on Visual Studio. Signal treatment and pore detection techniques are further detailed in Supplemental Material, where methods to identify and measure the different conductive modes are also discussed.

Summary of physical quantities.

variable	variable name	units
ℓ	membrane thickness	nm
\mathcal{D}	diffusion coefficient	$\text{m}^2 \cdot \text{s}^{-1}$
S	membrane area	m
P_m	permeability	$\text{m} \cdot \text{s}^{-1}$
U_m	barrier height	joule
K_w	partition coefficient	dimensionless
V	applied potential	V
u	reduced potential	dimensionless
I_c	intrinsic current	pA
i_c	intrinsic current density	$\text{mA} \cdot \text{m}^{-2}$
I_p	pore current	pA
D_p	pore diameter	nm
τ	detection response time	ms
τ_p	pore opening time	ms
N_s	pore opening frequency	s^{-1}
f_p	attempt frequency	s^{-1}
C_s	membrane capacitance	F

ACKNOWLEDGMENTS. E.J.L. thanks the Franco-German University and the French Ministry of High Education for a PhD grant. The team is beholden to M. Basler for the development of equipment allowing fast lipid hydroperoxidation and to C. Gicquel and L. Fayolle for help with pore data analysis. Y. Moskalenko is gratefully acknowledged for support with the protocol for lipid synthesis.

1. D Miklavčič, G Serša, *Handbook of Electroporation*. (Springer International Publishing) No. v. 1, (2020).
2. T Kotnik, L Rems, M Tarek, D Miklavčič, Membrane electroporation and electroporation: mechanisms and models. *Annu. review biophysics* **48**, 63–91 (2019).
3. A Hemmerle, G Fragneto, J Daillant, T Charitat, Reduction in tension and stiffening of lipid membranes in an electric field revealed by x-ray scattering. *Phys. Rev. Lett.* **116**, 228101 (2016).
4. RA Böckmann, BL De Groot, S Kákorin, E Neumann, H Grubmüller, Kinetics, statistics, and energetics of lipid membrane electroporation studied by molecular dynamics simulations. *Biophys. journal* **95**, 1837–1850 (2008).
5. BN Ames, MK Shigenaga, TM Hagen, Oxidants, antioxidants, and the degenerative diseases of aging. *Proc. Natl. Acad. Sci.* **90**, 7915–7922 (1993).
6. R Itri, C Marques, M Baptista, *The Giant Vesicle Book*. (CRC Press, Boca Raton, FL), pp. 473–487 (2019).
7. G Weber, et al., Lipid oxidation induces structural changes in biomimetic membranes. *Soft Matter* **10**, 4241–7 (2014).
8. M Paez-Perez, et al., Directly imaging emergence of phase separation in peroxidized lipid membranes. *Commun. Chem.* **6**, 15 (2023).
9. Y Guo, VA Baulin, F Thalmann, Peroxidised phospholipid bilayers: insight from coarse-grained molecular dynamics simulations. *Soft matter* **12**, 263–271 (2016).
10. P Siani, R de Souza, L Dias, R Itri, H Khandelia, An overview of molecular dynamics simulations of oxidized lipid systems, with a comparison of elba and martini force fields for coarse grained lipid simulations. *Biochimica et Biophys. Acta (BBA)-Biomembranes* **1858**, 2498–2511 (2016).
11. R De Rosa, F Spinozzi, R Itri, Hydroperoxide and carboxyl groups preferential location in oxidized biomembranes experimentally determined by small angle x-ray scattering: Implications in membrane structure. *Biochimica et Biophys. Acta (BBA)-Biomembranes* **1860**, 2299–2307 (2018).
12. AP Schroder, E Zaitseva, CM Marques, JC Behrends, Voltage-dependent formation of stable, ion conductive pores in suspended lipid bilayers from oxidized lipids. *Biophys. J.* **112**, 219A (2017) 58th Annual Meeting of the Biophysical-Society, San Francisco, CA, FEB 15-19, 2014.
13. B Hille, *Ionic Channels of Excitable Membranes*. (Sinauer Associates, Sunderland, MA), 3rd edition, (2001).
14. C Hanneschlaeger, A Horner, P Pohl, Intrinsic membrane permeability to small molecules. *Chem. reviews* **119**, 5922–5953 (2019).
15. SW Kowalczyk, AY Grosberg, Y Rabin, C Dekker, Modeling the conductance and dna blockade of solid-state nanopores. *Nanotechnology* **22**, 315101 (2011).
16. DE Goldman, Potential, impedance, and rectification in membranes. *The J. general physiology* **27**, 37–60 (1943).
17. AL Hodgkin, B Katz, The effect of sodium ions on the electrical activity of the giant axon of the squid. *The J. physiology* **108**, 37 (1949).
18. JE Hall, C Mead, G Szabo, A barrier model for current flow in lipid bilayer membranes. *The J. Membr. Biol.* **11**, 75–97 (1973).
19. B Fuks, F Hombler, Permeability and electrical properties of planar lipid membranes from thylakoid lipids. *Biophys. journal* **66**, 1404–1414 (1994).
20. H Junqueira, et al., Molecular organization in hydroperoxidized popc bilayers. *Biochimica et Biophys. Acta (BBA)-Biomembranes* **1863**, 183659 (2021).
21. KC Melikov, et al., Voltage-induced nonconductive pre-pores and metastable single pores in unmodified planar lipid bilayer. *Biophys. journal* **80**, 1829–1836 (2001).
22. M Winterhalter, W Helfrich, Effect of voltage on pores in membranes. *Phys. Rev. A* **36**, 5874 (1987).
23. WM Haynes, DR Lide, TJ Bruno, *CRC handbook of chemistry and physics*. (CRC press), (2016).
24. RW Glaser, SL Leikin, LV Chernomordik, VF Pastushenko, AI Sokirko, Reversible electrical breakdown of lipid bilayers: formation and evolution of pores. *Biochimica et Biophys. Acta (BBA)-Biomembranes* **940**, 275–287 (1988).
25. JT Sengel, MI Wallace, Imaging the dynamics of individual electropores. *Proc. Natl. Acad. Sci.* **113**, 5281–5286 (2016).
26. I Abidor, et al., Electric breakdown of bilayer lipid membranes: I. the main experimental facts and their qualitative discussion. *J. electroanalytical chemistry interfacial electrochemistry* **104**, 37–52 (1979).
27. KT Powell, JC Weaver, Transient aqueous pores in bilayer membranes: a statistical theory. *Bioelectrochemistry Bioenerg.* **15**, 211–227 (1986).
28. Z Vasilkoski, AT Esser, T Gowrishankar, JC Weaver, Membrane electroporation: The absolute rate equation and nanosecond time scale pore creation. *Phys. review E* **74**, 021904 (2006).
29. P Boonnoy, V Jarerattanachai, M Karttunen, J Wong-Ekkabut, Bilayer deformation, pores, and micellation induced by oxidized lipids. *The journal physical chemistry letters* **6**, 4884–4888 (2015).
30. T Heimburg, Lipid ion channels. *Biophys. chemistry* **150**, 2–22 (2010).
31. ZA Levine, PT Vernier, Life cycle of an electropore: field-dependent and field-independent steps in pore creation and annihilation. *The J. membrane biology* **236**, 27–36 (2010).
32. E Zaitseva, et al., Electrophysiology on channel-forming proteins in artificial lipid bilayers: Next-generation instrumentation for multiple recordings in parallel in *Patch Clamp Electrophysiology*. (Springer), pp. 67–92 (2021).
33. SH White, Analysis of the torus surrounding planar lipid bilayer membranes. *Biophys. journal* **12**, 432–445 (1972).

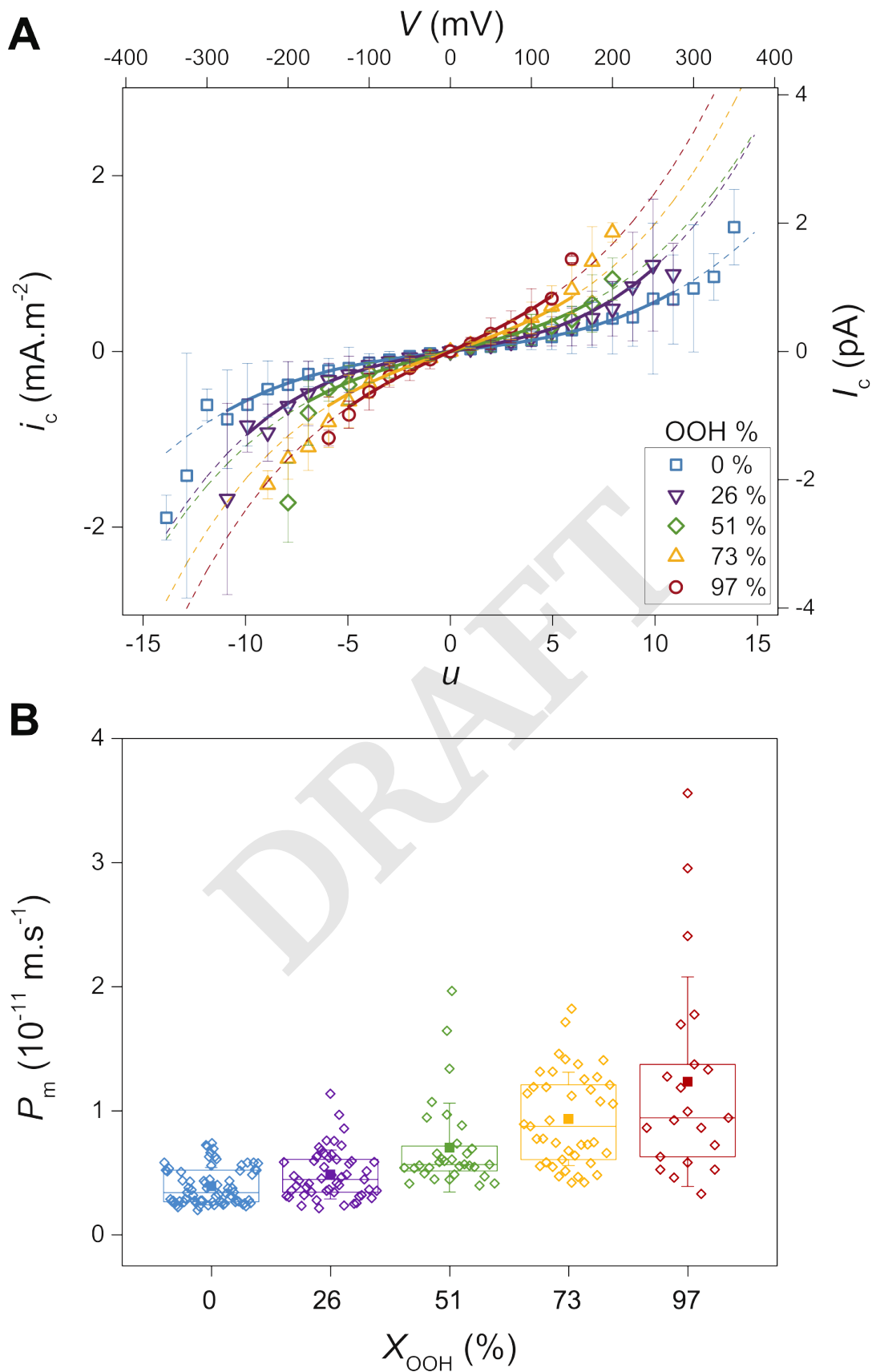


Fig. 3. Intrinsic membrane electropemeability. (A) $i_c - V$ characteristics in a pore-free membrane. Left axis measures current density, right axis expresses current across a patch of $42 \mu\text{m}$ diameter. X-axis displays normalized voltage units $u = eV/(k_B T)$, voltage is shown in top horizontal axis. Full lines drawn in the range where Eq. (1) adequately fits the data, dashed lines extrapolate the fit over the whole range as a guide to the eyes; error bars measure the standard deviation. (B) Permeability of POPC membranes as a function of X_{OOH} , the molar fraction of hydroperoxidized lipids. The data is displayed as box-plots representing the distribution of membrane permeability based on first quartile, median, mean (filled square symbol), third quartile, with whiskers showing standard deviation.

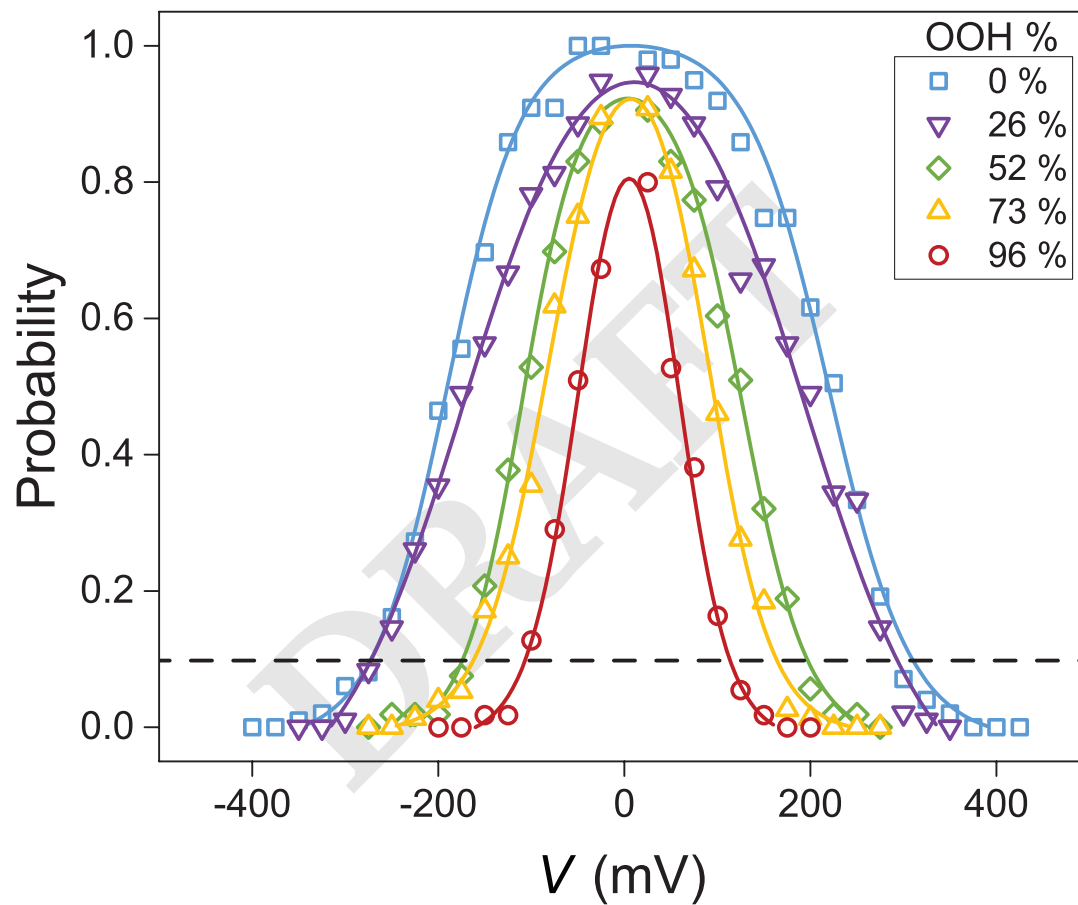


Fig. 4. Membrane probability to remain pore-free. Symbols represent the calculated probability; solid lines are a guide to the eyes. 10 % probability shown by dashed line.

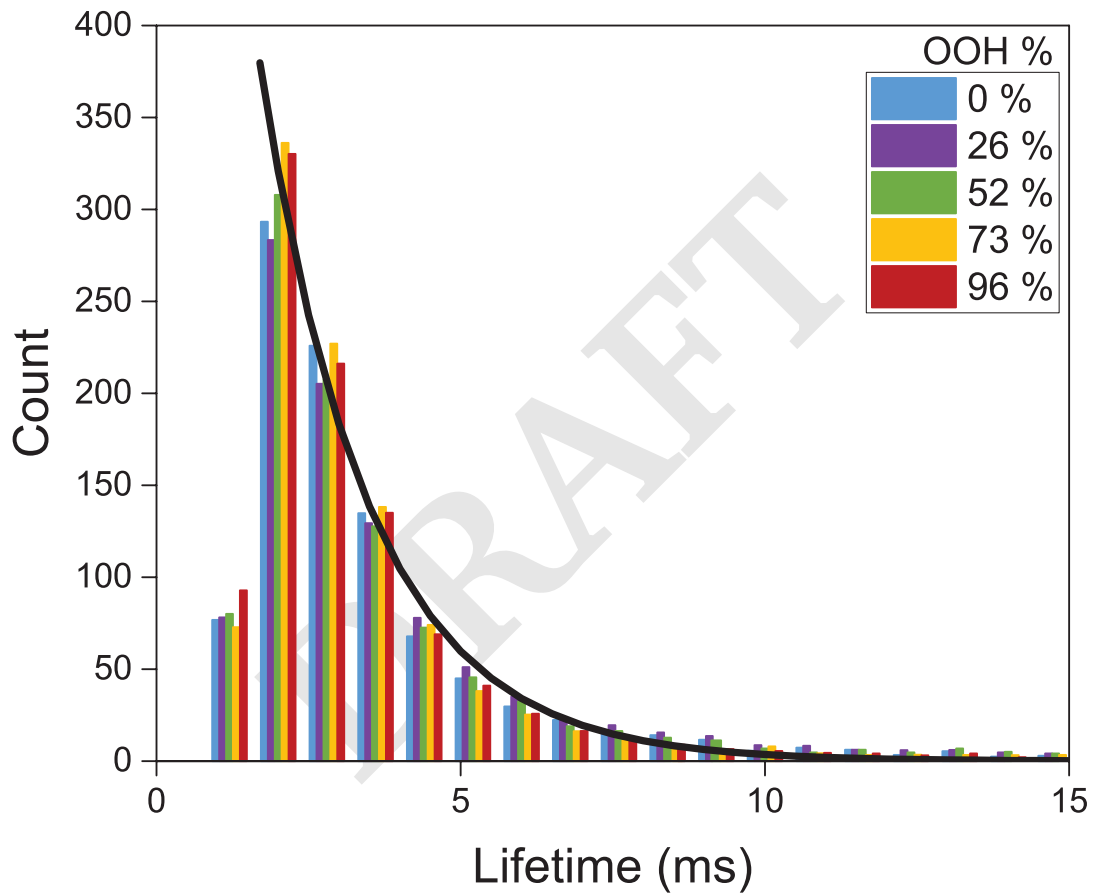


Fig. 5. Lifetime distribution of identifiable pores (bin=0.8 ms) normalized for 1000 pores. Solid line represents a single exponential fit.

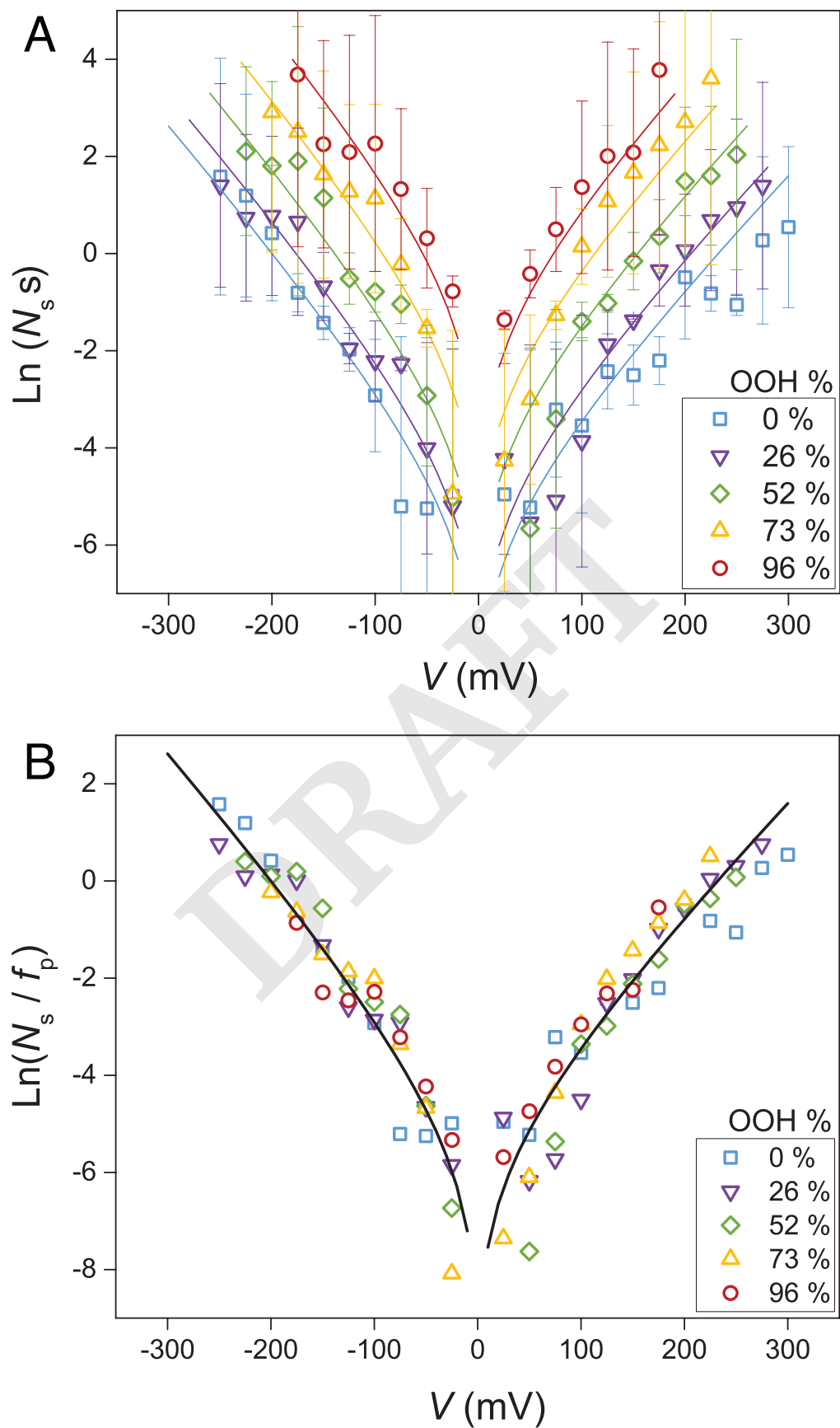


Fig. 6. (A) Average number of short lifetime pores opening per second as a function of voltage for the different hydroperoxidation degree of POPC membranes. Error bars represent standard deviation. Solid lines represent fits by Eq. 2. (B) Master curve obtained by normalizing N_s over f_p . Please note that Y-axis represent natural logarithm values.